PAPER

Check for updates

Highly efficient degradation of reactive black KN-B dye by ultraviolet light responsive ZIF-8 photocatalysts with different morphologies†

Le Gia Trung, [ID] ‡[a] Minh Kim Nguyen,‡[b] Thi Dieu Hang Nguyen,[c] Vy Anh Tran,[de] Jin Seog Gwag [ID] *[a] and Nguyen Tien Tran [ID] *[fg]

Zeolitic imidazolate framework ZIF-8, a type of metal–organic framework, has diverse applications in multiple catalytic fields due to its outstanding properties. Herein, ZIF-8 photocatalysts with three different morphologies (dodecahedral, pitaya-like, and leaf-like) are successfully synthesized under ambient conditions from zinc salts by altering the volume ratio of methanol and water used as a solvent. The as-synthesized ZIFs have high crystallinity with distinct BET surface areas. The experiments indicate that the ZIFs have high photocatalytic efficiency, in which the leaf-like structure (ZIF-8-F3) is the most efficient in the degradation of reactive black KN-B dye (RB5) under 365 nm UV irradiation. This is due to the efficient inhibition of electron–hole recombination or the higher migration of charge carriers in ZIF-8-F3, thus producing more reactive oxygen species, resulting in greater photocatalytic efficiency. At pH = 11, more than 95% of RB5 is degraded within 2 hours when using 1.0 g L^{-1} of ZIF-8-F3. Besides, the photocatalytic and kinetic performances of ZIF-8-F3 are also investigated by optimizing the pH, initial RB5 concentration, and dosage of the used catalyst. These ZIF-8-F3 plates have been shown to be a promising material with high photostability and effective reusability, beneficial to various potential applications in environmental remediation issues.

1. Introduction

Water pollution is one of the most serious environmental issues today, endangering both human health and animal life.[1] Accordingly, it is critical and essential to regulate and treat water sources. Water contamination may be due to a variety of causes, such as rapid urban development, chemical waste dumping, fertilizer run-off, radioactive waste discharge, and so on.[2] Moreover, in modern science, hundreds of emergent organic contaminants (EOCs) have been found in recent years, which have been greatly affecting water resources, including medicines, personal care items, industrial pollutants, *etc.*[3] Due to the physicochemical features of EOCS, such as easy dispersibility or solubility in water or high grade, it is almost impossible to eliminate them, even at low concentrations, if only using the conventional procedures of water treatment.[4] Additionally, many sources of inorganic compounds also cause implicit risks to the health and safety of humans, including carcinogenicity, mutagenicity, teratogenicity, or toxicity. Therefore, the proper procedures for wastewater purification are still a strategy and a challenge for scientists. In that, although coagulation and filtration methods have been extensively studied,[5] they do not appear to be completely optimized because the used facilities are rather large and complicated, with high maintenance costs.[6] Besides, how to completely convert pollutants into green components is still a great challenge right now. When the concern about energy and economization is particularly considerable, the adsorption and photocatalytic methods are fairly promising to remove contaminants.[7] In which adsorption is a surface and interfacial phenomenon with a common mechanism to effectively remove inorganic and organic pollutants in industrial wastewater. Adsorption can also occur in various environments, such as solid–liquid, solid–gas, liquid–liquid, and liquid–gas. In addition, adsorption has many advantages: simple design, low

[a]Department of Physics, Yeungnam University, Gyeongsan, Gyeongbuk 38541, Republic of Korea. E-mail: sweat3000@ynu.ac.kr

[b]College of Pharmacy, Chungnam National University, Yuseong, Daejeon 34134, Republic of Korea

[c]The University of Da Nang, University of Science and Technology (DUT), 54 Nguyen Luong Bang, Da Nang, 550000, Vietnam

[d]Institute of Applied Technology and Sustainable Development, Nguyen Tat Thanh University, Ho Chi Minh City 700000, Vietnam

[e]Faculty of Environmental and Food Engineering, Nguyen Tat Thanh University, Ho Chi Minh City 700000, Vietnam

[f]Center for Advanced Chemistry, Institute of Research and Development, Duy Tan University, 03 Quang Trung, Da Nang, 550000, Vietnam. E-mail: trannguyentien@duytan.edu.vn

[g]Faculty of Natural Sciences, Duy Tan University, 03 Quang Trung, Da Nang, 550000, Vietnam

† Electronic supplementary information (ESI) available. See DOI: https://doi.org/10.1039/d2ra08312d

‡ These authors contributed equally to this work and are co-first authors.

equipment investment, easy operation, wide pH range, and high performance.[8] Therefore, the adsorption process using solid adsorbents displays great potential as one of the most efficient methods for industrial wastewater treatment. There are many technologies used in wastewater decontamination, e.g., membrane filtration, precipitation, etc.[9] Among the possible methods, the photocatalytic technique is fairly effective because of its simple process and green technology.[10–14] Additionally, this method has been rapidly used in various applications, such as CO_2 reduction, water splitting, etc. Consequently, researchers have been studying and looking for new adequate materials that can be used to make better adsorbents or photocatalysts to get rid of pollutants.[15,16]

In recent years, nanomaterials with low-dimensional structures have been widely used as a new type of promoted material due to their superior physicochemical properties for many potential applications, such as fluorescent probes, inorganic membranes of gibbsite platelets, anisotropic films, etc.[17–19] A metal–organic framework (MOF) is a porous material with one- (1D), two- (2D), or three-dimensional (3D) structures made up of metal ions or clusters coordinated to organic ligands. That has been extensively studied as an interesting material in research and technology.[20] In general, the geometry and physicochemical properties of MOF building units can be changed due to the synthesis procedures and conditions, hence allowing for a synergistic combination of their features.[21] As well-known, MOFs with pore structures have a large surface area, excellent stability in polymetallic complexes, and good compatibility with polymers.[22] Indeed, MOFs are also outstanding materials to eliminate hazardous metals, EOCs, or other contaminants from wastewater due to their structural variety and unique characteristics.[23] Similarly, zeolitic imidazolate framework (ZIF) materials are also a type of MOF with a zeolite skeleton using zinc (Zn) or cobalt (Co) as metal sites and imidazole as organic ligands.[24] These ZIFs reveal that the thermal and chemical stability are higher than other common MOFs.[25] Based on those excellent features, ZIFs have been widely used in the science and industry fields since 2006.[26]

ZIF-8, as a common material for ZIFs, was first prepared by Chen et al. with a designation model of MAF-4.[27] Afterward, Yaghi et al. comprehensively investigated MAF-4 and named it ZIF-8.[28] ZIF-8 has the chemical formula $Zn(2\text{-MIM})_2$, which consists of 2-methylimidazole (2-MIM) and the metallic site zinc.[26,29] In addition, the synthetic procedure of ZIF-8 is rather diverse and simple when compared to other MOFs. ZIF-8 also shows superior chemical and thermal resistance based on its strong link structure. Furthermore, ZIF-8 has good morphological stability up to 500 °C. ZIF-8 may retain its crystalline structure and microstructure even when being immersed in various solutions such as water or organic solvents.[29] ZIF-8 has easily tunable pore sizes and topologies, which makes it adaptable. ZIF-8 materials have been produced in several forms, such as powder, particle, membrane, and platelet, and are widely applied in diverse vital sectors.[23–26,30,31] Reactive Black KN-B (RB5) is one of the most common reactive azo dyes, also named Remazol Black B, with a structure of two azo bonds (–N=N–).[32] RB5 is broadly used in the textile industry for dye

processes. Alarmingly, more than 50% of the dyes used in the textile industry are azo dyes due to their useable features such as bright and high-intensity colors, fastness, easy preparation, low cost, high solubility and stability.[33] Therefore, the degradation of RB5 is essential to protect the environment and human health. A decade ago, several catalysts were applied to degrade RB5, such as ZnO, TiO_2, and ZnS.[33–35]

Here, we successfully synthesize ZIF-8 materials with three different morphologies at room temperature by using a simple in situ solvent-induced growth method, and then use them in the photocatalytic degradation of the RB5 dye. Interestingly, 2D leaf-like laminated ZIF-8 material is superior to the others in the photodegradation of RB5. The results are demonstrated by employing SEM, thermogravimetric analysis, electrochemical impedance spectroscopy, ultraviolet-visible diffusion reflectance spectroscopy, photoluminescence, photocurrent tests, and the influence of various scavengers. So far as we know, this is the first study that looks at how the structure of ZIF-8 materials affects the photocatalytic degradation of RB5 by using materials with different shapes.

2. Experimental section

2.1 Materials

Zinc nitrate hexahydrate ($Zn(NO_3)_2 \cdot 6H_2O$, 99%) and 2-methylimidazole (2-MIM, $C_4H_6N_2$, 99%) were purchased from Sigma Aldrich, USA. Reactive Black KN-B (RB5, dye) was provided by Bomei Co. (Anhui, China). Methanol (99.8%) was acquired from Daejung Co. (Korea). The MAX Ultra 370 Series was used in the study to produce deionized (DI) water. All used reagents were of analytical grade and were employed directly as obtained without additional treatment. The formation of ZIF-8 and the chemical structure of 2-MIM and RB5 were represented in Scheme 1.

2.2 The preparation of ZIF-8

ZIF-8 materials with different morphologies were synthesized at room temperature by using a slightly modified process described in the literature.[36,37] In typical, solution A contains 2.0 mmol of $Zn(NO_3)_2 \cdot 6H_2O$ and 30 mL of the solvent, solution B contains 12.0 mmol of 2-MIM and 100 mL of the solvent. The solvent is a mixture of methanol and water with target volume ratios. Two solutions were mixed together and magnetically agitated vigorously for 30 min at room temperature. The post-agitation milky suspension was kept undisturbed for 12 h (i.e., no stirring). Following that, the resultant white sediments were collected and washed several times with methanol, and then completely dried overnight in a vacuum oven (60 ± 1 °C). By varying the volume ratio of methanol and water ($V_{methanol} : V_{water}$) as 1 : 2, 1 : 3.5, and 0 : 1, three morphologies of ZIF-8 were fabricated with the following shapes: 3D rhombic dodecahedron (ZIF-8-F1), pitaya (ZIF-8-F2), and 2D leaf (ZIF-8-F3), respectively.

2.3 Characterization

The following paths were used to acquire the characteristics of the sample and analytical patterns: X-ray diffractometry (XRD; M18XHF-SRA; Mac Science, Japan) was used to assess the phase
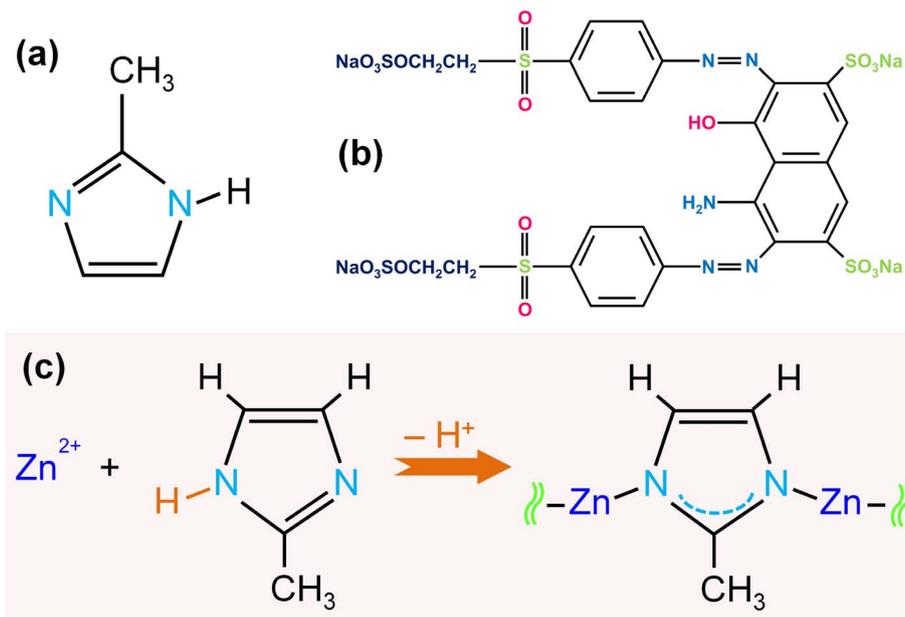
Scheme 1 Chemical structures of (a) 2-MIM and (b) RB5. (c) The formation of ZIF-8.

purity and crystallographic structure of materials in a range of 5–40° with a scanning rate of 5° min^{-1}. Scanning electron microscopy (SEM, Leo-Supra 55, Carl Zeiss STM, Germany) was used to observe the morphologies of photocatalysts. The analyses for the photocatalytic efficiency were studied using ultraviolet-visible diffusion reflectance spectroscopy (UV-Vis DRS; Cary 50-UV Vis Spectrophotometers; Varian Inc., USA) in a wavelength range of 200–600 nm. Photoluminescence (PL) spectroscopy was taken on a Synergy H-1M Multi Microplate Reader (BioTek Instruments Korea Ltd., Korea). Chemical composition of the synthesized ZIF-8 materials was examined using X-ray photoelectron spectroscopy (XPS, Thermo ESCALAB 250Xi, USA) with an Al Kα anode (X-ray source, 300 W). The specific surface area and porosity analysis were collected from N$_2$ adsorption–desorption at 77 K (Belsorp-mini instrument, BEL Japan Inc.). Infrared spectra of the as-prepared samples were recorded in a range of 500–4000 cm^{-1} using a Fourier transform infrared spectrometer (FTIR, Nicolet 6700). Thermogravimetric analysis (TGA) was performed on a thermal analyzer (PerkinElmer TGA-8000) from room temperature to 700 °C under a nitrogen atmosphere with a heating rate of 10° C min^{-1}. Zeta potential measurements were recorded by a Zetasizer 2000 (Malvern, UK) to determine the surface charges of the ZIF-8 samples.

The electrochemical impedance spectroscopy (EIS) data and transient photocurrent (PC) density were measured by a Biologic SP 200 in a 0.5 M Na$_2$SO$_4$ electrolyte solution. The EIS analysis was carried out in a frequency range of 0.01 to 1 MHz. The PC measurement was taken in full-spectrum light (MaX 303, 150 W) with a light intensity of 50 mW cm^{-2}. The as-prepared catalysts were embedded on ITO glass substrates (as a working electrode) by using a simple drop-casting process. Under the aforementioned light source, a platinum counter electrode and an Ag/AgCl (saturated KCl) electrode were utilized

as the counter and reference electrodes, respectively. The photocatalytic and trapping experiments were performed in a similar manner. In these tests, all scavengers were used at an equivalent concentration (1.0 mM). In typical, ethylenediaminetetraacetic acid (EDTA) was employed as a probe for holes (h$^+$), potassium persulfate (K$_2$S$_2$O$_8$) was used to induce electrons (e$^-$), 1,4-benzoquinone (BQ), and isopropyl alcohol (IPA) were applied as radical scavengers for superoxide radical anions ($^\bullet$O$_2^-$) and hydroxyl radicals ($^\bullet$OH), respectively.[38–40] As is known, terephthalic acid (C$_8$H$_6$O$_4$, 98%, from Sigma Aldrich, USA) has been used as a probe for $^\bullet$OH radicals in aqueous solutions. This acid tends to interact with $^\bullet$OH radicals to generate 2-hydroxyterephthalic acid at an excitation wavelength of 300 nm.[15] Measuring the concentration of formed 2-hydroxyterephthalic acid could quantify the $^\bullet$OH radicals in the samples. The spin-trapping electron paramagnetic resonance (EPR) spectra were collected 30 s after the introduction of the respective photocatalysts via an X-band EPR spectrometer (MS 5000, Magnetek, Germany). The EPR measurements were prepared by dispersing 50 mg of ZIF-8s into a 25 mM DMPO (5,5′-dimethyl-1-pyrroline-N-oxide) solution for DMPO-$^\bullet$OH, or 50 mL methanol for DMPO-$^\bullet$O$_2^-$, respectively.

2.4 The dye degradation procedure and evaluation of photocatalytic activity

The photodegradation of RB5 dye was used to test the photocatalytic performance of three ZIF-8 materials under ultraviolet (UV) illumination in the open air at room temperature. In a typical experiment, 50 mg of each ZIF-8 photocatalyst was mixed with 50 mL of aqueous RB5 solution (20 mg L^{-1}). The photocatalytic study was carried out using a 100 mL clamp, and a water circulation gear was used to keep the temperature constant at 25 °C. A commercial xenon arc lamp (300 W,

Newport Optical Filters, Korea) joined with monochromatic light filters to yield a desired irradiation wavelength (365, 500, and 600 nm) was parallel placed outside the beaker. The distance between the beaker containing the explored solution and the light generator was 10 cm. About 5 mL of the sample from the glass beaker was taken at 20 minute intervals and then centrifuged at 5000 rpm for 5 min to recover the photocatalyst granules. A UV-Vis spectrophotometer was used to evaluate the obtained supernatants at a wavelength of 598 nm. The pH value of the solution can be adjusted by using HCl (0.1 M) or NaOH (0.1 M).

The dye photodegradation efficiency η of the catalysts was determined by a formula:

$$\eta = (1 - C/C_0) \times 100 \tag{1}$$

where C_0 and C are the concentrations of the RB5 dye (mg L^{-1}) before and at a certain time t of UV irradiation, respectively. The rate constant for the photocatalytic reactions was calculated using the Langmuir–Hinshelwood kinetic model with an equation as:[41]

$$-\ln(C/C_0) = kt \tag{2}$$

where C_0 and C are the concentrations of the RB5 dye before and at a certain time t of UV irradiation, respectively. k is the pseudo-first-order rate constant. The concentration of samples was interpolated from the Beer–Lambert law.[42] All degradation reactions use the pseudo-first-order kinetic model. To achieve high reliability, all experiments were repeated three times, and the results were obtained as the average of the samples.

3. Results and discussion

3.1. Characterization of the ZIF-8 photocatalysts

SEM images in Fig. 1 show the morphologies of three ZIF-8 materials before and after three cycles of RB5 photodegradation. The images obviously display that the different volume ratios of methanol and water in the solvent have a substantial impact on the geometry of the obtained products. This morphological transformation is clear when the water content in the solvent increases from 66.7% to 100%. ZIF-8, prepared at a methanol/water volume ratio of 1 : 2, is 3D rhombic dodecahedral particles with a uniform size, named ZIF-8-F1 (Fig. 1a-i). The mean geometric length of the dodecahedral ZIF-8 facets is 450 ± 35 nm. The pitaya-like ZIFs, named ZIF-8-F2, are obtained at a methanol/water volume ratio of 1 : 3.5 with a particle size of 1.8 ± 0.4 μm (Fig. 1b-i). When water is employed as the main medium ($V_{methanol} : V_{water} = 0 : 1$), 2D leaf-like ZIFs are achieved (ZIF-8-F3) as shown in Fig. 1c-i. These ZIF-8 leaves have a smooth surface with a rather large size of several microns but only a thickness of 200 nm. ZIF-8-F2 is attributed to an intermediate product between 3D ZIFs and 2D ZIFs with spherical and leaf-like structures.[37] Interestingly, even after three cycles of RB5 photocatalytic degradation, the architectures of all three ZIF materials did not change significantly when compared to the initial ZIF-8 samples (Fig. 1a-ii, b-ii and c-ii). As a result, the ZIF-8 crystals are almost homogeneous and stable.

Fig. 2a shows the XRD spectra of the as-synthetic ZIFs. Both the two ZIF-8 materials of dodecahedral shape (F1) and pitaya (F2) have similar XRD patterns, indicating their same lattice structures.[29] Both these ZIF-8 samples revealed major characteristic peaks at 7.3, 10.8, 12.9, 14.8, 16.7, and 18.2°, which corresponded to the (011), (002), (112), (022), (013), and (222) planes of the ZIF-8 crystals, respectively, while the minor peaks after 20° are negligible (JCPDS 00-062-1030).[43] Furthermore, the clear and strong peaks show that two F1 and F2 materials have high crystallinity and a space group ($I\bar{4}_3m$) that matches the previously simulated XRD patterns.[44] On the contrary, leaf-like ZIFs have a distinct XRD pattern due to different 2D lattice structures (JCPDS no. 01-1136).[45] This could be the reason that its surface area is much lower than the others. Therefore, it is observed that the 2D ZIFs clearly contain distinct cushion-shaped space groups (*Cmce*) as opposed to the round-shaped
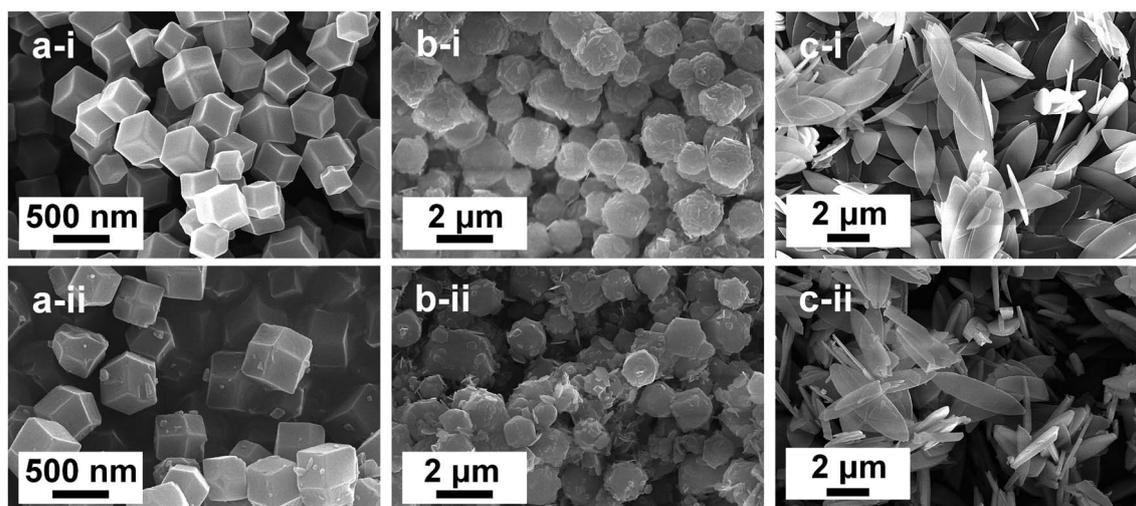

Fig. 1 SEM images of three ZIF-8 materials: (a) rhombic dodecahedral ZIF-8-F1, (b) pitaya-like ZIF-8-F2, and (c) leaf-like ZIF-8-F3 before (i) and after (ii) three cycles of RB5 photodegradation.
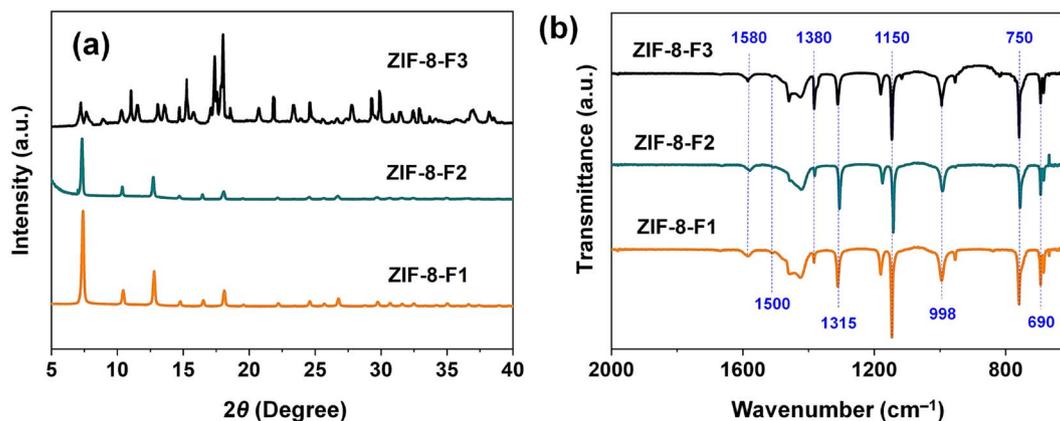
Fig. 2 (a) XRD patterns and (b) FTIR spectra of three as-synthetic ZIF-8 samples.

spaces of ZIF-8-F1. The as-synthetic ZIFs are further characterized by FTIR, shown in Fig. 2b, to investigate their chemical compositions. It plainly shows that three materials from ZIF-8 have similar FTIR spectra. This might be elucidated since the assembled forces of 2-MIM molecules with zinc atoms in ZIFs are the same.[46] In typical, the stretching vibration at 1580 cm^{-1} is attributed to the C=N bonds. The bands between 1500–1380 cm^{-1} can be assigned to the stretching vibration of the imidazole rings, whereas the bending vibrations of the imidazole rings regard the peaks in 1315–1150 cm^{-1}. The peaks at 998 and 750 cm^{-1} are responsible for the bending vibrations of C–N and C–H bonds, respectively. Lastly, the signal at 690 cm^{-1} is related to the out-of-plane bending of the imidazole ring. Overall, upon SEM and the characterizations of XRD/FTIR in Fig. 1 and 2, they definitely confirm that the as-synthetic materials are ZIF-8 with different desired morphologies.

In general, photocatalytic reactions tend to happen on the outer surface of catalysts. Besides, the activity of catalysts is closely related to the surface area and the porosity of the catalyst. The Brunauer–Emmett–Teller (BET) specific surface area and pore structure of three as-prepared ZIFs can also be studied through the N$_2$ adsorption–desorption isotherms method. As

seen in Fig. 3a, both the dodecahedral and pitaya-shaped ZIFs are type I isotherms with high N$_2$ adsorption contents at low pressure due to their microporous and mesoporous architectures, with a volume of 1.10 and 0.63 cm^3 g^{-1}, respectively. Typically, their micropore and mesopore sizes are measured respectively at 0.62 and 3.80 nm for ZIF-8-F1; 0.53 and 3.50 nm for ZIF-8-F2 (Fig. 3b). However, the clear increase at high pressure may be assigned to the crystal stacking of the textural macrospores.[47] On the contrary, leaf-like ZIFs reveal low N$_2$ adsorption content along with a poor porous structure and a low pore volume of 0.15 cm^3 g^{-1}. In addition, its pore size distribution is low. That might result from its 2D layered organizations with a bigger size, higher density, and fewer channel. The BET surface area of the as-synthetic ZIF-8 materials (F1, F2, and F3) is 1308.2, 683.7, and 62.4 m^2 g^{-1}, respectively (see Table 1).

XPS analysis is a useful technique to investigate the chemical compositions and oxidation states of the atoms.[48] The peaks in the XPS spectra of three ZIF-8 materials before and after three cycles of RB5 photodegradation (see Fig. S1 in ESI†) still maintained their positions (i.e., insignificant shifts). Consequently, the synthesized ZIF-8 photocatalysts are stable after
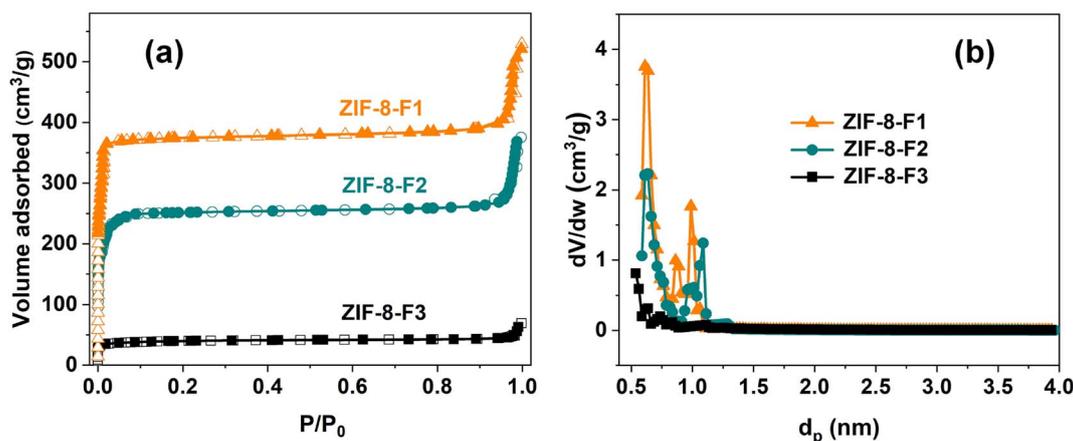

Fig. 3 (a) N$_2$ adsorption–desorption isotherms of three as-synthetic ZIF-8 materials and (b) their corresponding pore size distributions.

Table 1 Structure characteristics of the three ZIF-8 materials

Material	S_{BET} (m^2 g^{-1})	Pore size (nm)	Pore volume (cm^3 g^{-1})	Particle size (nm)
Dodecahedral (F1)	1308.2	0.62	1.10	450 ± 35
Pitaya-like (F2)	683.7	0.53	0.63	1800 ± 400
Leaf-like (F3)	62.4	0.12	0.15	3500 ± 700
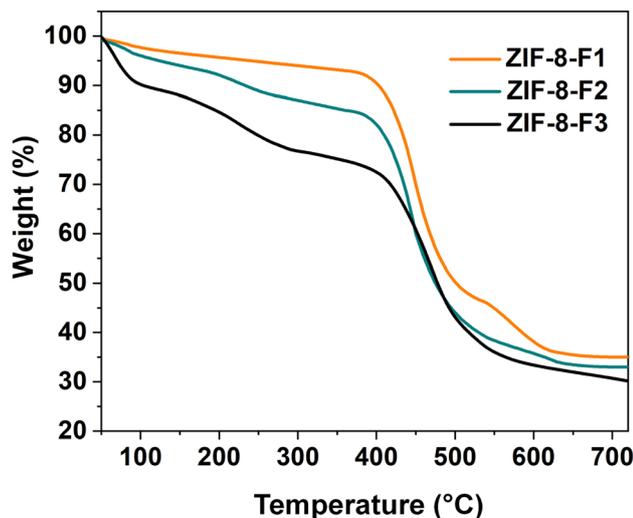
Fig. 4 TGA curves of three as-synthetic ZIF-8 samples at a heating rate of 10 °C min^{-1}.

three degradation cycles of RB5 dye solution. Thermal stability is used to examine the quality of the samples at high temperatures.[42] Thermogravimetric curves of three ZIF-8 materials are shown in Fig. 4. The main frameworks of ZIFs are inherited from organic compounds. Consequently, they are thermally unstable, and their TGA curves reveal three major mass losses. The initial mass loss for all samples started at 65 °C and was assigned to the vaporization of residual moisture and physically absorbed solvents (i.e., water and methanol) in the ZIF-8 materials.[49] The weight loss of the leaf-like ZIF-8-F3 material was the highest at approximately 10% due to the large absorption of solvents on this sample surface or between adjacent layers. The second weight reduction at 265 °C was attributed to the carbonization of imidazole molecules in ZIF-8 pores.[28] Meanwhile, a majority of the mass loss occurred at 475 °C with a significant reduction for the F1, F2, and F3 materials of 43, 49, and 51%, respectively. That was related to the decomposition of organic linkers in the ZIF-8 crystals. After 600 °C, the mass was reduced negligibly. Based on the leaf-like morphology of ZIF-8-F3, its thermal stability was the lowest, with a high mass loss of approximately 71% up to 700 °C.

3.2. Experiments on the photocatalytic degradation of RB5 dye

3.2.1 Photocatalytic performances. To test the photocatalytic efficiency of three as-synthetic ZIF-8 materials for the degradation of RB5 dye, 50 mg of each ZIF-8 was mixed in

a sealed beaker with 50 mL of the aqueous RB5 solution (20.0 mg L^{-1}) at pH = 7.0. The beaker was kept undisturbed in the dark for 50 min, and then irradiated under UV illumination (365 nm) at ambient conditions for various periods (20, 40, 60, 80, 100, and 120 min). The reduction in the absorbance intensity indicates that the RB5 dye was absorbed into the catalysts (Fig. 5). As is well-known, the pseudo-first-order kinetic model is efficiently used for photocatalytic degradations.[15] Consequently, the slopes of the fitting straight lines based on the graph of $-\ln(C/C_0)$ vs. time,[41] seen in eqn (2), correspond to their first-order rate constants.

The absorption spectrum of RB5 before the photocatalytic degradation shown in Fig. 5a (black curve, origin) reveals a characteristic peak at 598 nm in the visible band, which corresponds to a chromophore with a long conjugated π-system linked by two azo groups (–N=N–).[50] Also, this peak is used to evaluate the decolorization of the dye solutions. Indeed, the absorbance intensities of RB5 with the presence of photocatalysts decreased slightly in the dark but rapidly under UV illumination (Fig. 5a–c), suggesting that the chromophoric group and conjugated azo system in RB5 were broken. In addition, their intensities decreased nearly uniformly over time, implying that the catalysis of ZIF-8 materials has high stability in the degradation process. Whereas RB5 was degraded negligibly in the absence of ZIFs, even in the dark and in UV light of 1% and 5%, respectively (Fig. 5d), indicating its self-photolysis. Among ZIFs, for ZIF-8-F3, RB5 was decomposed at least in the dark at 6% for 50 min, while the highest by UV illumination was at 91% for 120 min (Fig. 5e), and the others were 87% (ZIF-8-F1) and 73% (ZIF-8-F2) under UV light (see Table 2). The catalytic turnover number (CTN), i.e., the UV/dark proportion, is an important factor in evaluating the absorbance proportion of materials in various conditions.[51] The CTNs of three ZIFs are calculated to be 3.69 (F1), 6.28 (F2), and 14.25 (F3). Based on the obtained results, it plainly proves that the 2D leaf-like ZIF-8 materials have the most effective photocatalysis for the degradation of RB5 dye under UV conditions. This might be based on the selective adsorption of ZIF-8-F3 to only RB5 dye. The photodegradation rate constant k of three ZIFs is, respectively, 0.020 (F1), 0.011 (F2), and 0.019 (F3) min^{-1} (Fig. 5f).

According to the obtained results in Fig. 5, the leaf-like ZIF-8-F3 materials exhibited faster RB5-dye adsorption than the others in the initial stage under UV irradiation, which might be related to the higher isoelectric point (pH$_{IEP}$) than the other two ZIF-8s (see Fig. S2†). This higher pH$_{IEP}$ value allows for more interaction between charge carriers. Furthermore, the surface charges of the photocatalyst can also be determined by measuring the zeta potential at different pH values to
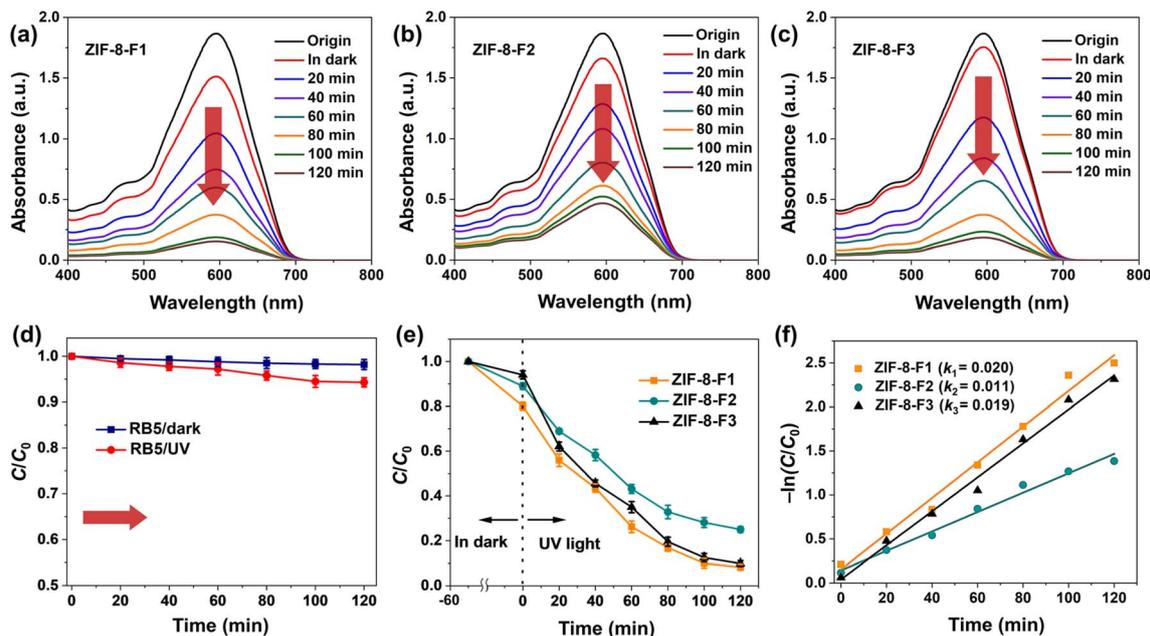
Fig. 5 (a–c) UV-Vis spectra by time for the RB5 degradation in the absence or presence of different ZIF-8 photocatalysts under two conditions: in the dark and under UV irradiation. (d) The photolysis of RB5 dye in the dark and UV light. (e) The plot of C/C_0 vs. time for the RB5 degradation with three ZIF-8 samples and (f) their corresponding models of pseudo-first-order kinetics.

understand the effect of pH on the photocatalytic process. It is known that the absorbent surface charge may be positive or negative if the pH value of the solution is lower or higher than pH_{IEP}, respectively.[48] Fig. S2† shows that the pH_{IEP} values of three ZIF-8s are approximately 10.3 (F1), 9.5 (F2), and 11.2 (F3); hence, the surface charge of the three samples is positive when the used pH of the solution is 7.0.

3.2.2 Optical and photoelectrochemical properties. In general, the electronic behavior of materials may be identified by UV-Vis measurements and photoluminescence (PL). Therefore, the optical properties of three ZIF-8 samples can also be explored through UV-Vis DRS and PL. In addition, photoelectrochemical tests such as EIS, photocurrent (PC), and the influence of various scavengers can demonstrate the plausible

Table 2 Comparison of the RB5 photodegradation efficiency η of three ZIF-8s with other materials

Material	Light source	Time (min)	η (%)	Ref.
N-doped TiO$_2$	Visible light	360	88	52
Mil-125(Ti)/CNT	UV	180	59	53
CF@ZIF-8	Visible light	180	89	54
TiO$_2$	UV	300	89	55
ZnO (pH = 11)	UV	60	92	56
SrTiO$_3$/CeO$_2$	UV	300	99	57
Ag$_3$PO$_4$ (pH = 11)	Visible light	120	90	58
WO$_3$/g-C$_3$N$_4$ (pH = 2)	Solar light	90	99	59
Reduced graphene oxide	UV	60	49	60
ZIF-8-F1	**UV**	**120**	**87**	**This work**
ZIF-8-F2	**UV**	**120**	**73**	**This work**
ZIF-8-F3	**UV**	**120**	**91**	**This work**

photocatalytic mechanism of ZIF-8 for the photodegradation/decolorization of RB5 dye.

Fig. 6a shows the characteristic absorption spectra of the as-synthetic ZIF-8 materials. Their UV-Vis DRS bands expand in the UV region (<400 nm) but are practically characterless in the visible region. Three ZIFs, including ZIF-8-F1, ZIF-8-F2, and ZIF-8-F3, exhibit a strong absorption of UV irradiation at *ca.* 218, 216, and 220 nm, respectively. That is attributed to the π–π* transition of aromatic C=C bonds in organic ligands[42] or the excitonic absorption of electron–hole pairs in ZIF-8.[61] This indicates that all ZIFs may have excellent UV photocatalytic features. Besides, the humped absorption edge is revealed at approximately 281 nm (F1), 282 nm (F2), and 273 nm (F3), which is assigned to the interactions of solvent molecules (*i.e.*, water or methanol) with the ZIF-8 framework.[62] The absorbance intensity of leaf-like ZIF materials is larger than the others by *ca.* 19%, indicating that ZIF-8-F3 can absorb the UV region stronger than the others. In addition, the increased intensity in the UV region may be due to the charge transfer from the valence band (VB) to the conduction band (CB).[25,38] The band gap energy plays a crucial role in determining the optical properties of materials. The mathematical equation of this energy can be expressed according to the Kubelka–Munk formula as: $\alpha h\nu = A(h\nu - E_g)^2$,[63] where α is the absorbance, h is the Planck constant, ν is the frequency of light, A is the proportionality constant, and E_g is the bandgap energy. The E_g value is determined following the Tauc method *via* the graph of $(\alpha h\nu)^{1/2}$ *versus* $h\nu$,[15] with the abscissa intercept of an elongated tangential vector from the linear region of the curve (inset in Fig. 6a). Consequently, the indirect bandgaps (E_g) of ZIF-8-F1, ZIF-8-F2, and ZIF-8-F3 are interpolated to be approximately 4.65, 4.89, and 4.15 eV,

Fig. 6 (a) UV-Vis DRS and (inset) Kubelka–Munk transformed DRS of ZIF-8 materials. (b) PL spectra of three ZIF-8 samples at an excitation wavelength of 310 nm.

respectively. The bandgap of ZIF-8-F3 is the minimum, implying that the photocatalytic efficiency may be the best. This result is suitable for the demonstrations in Fig. 5 and Table 2.

Photoluminescence spectroscopy is one of the effective approaches to probing the electronic structure of materials. In addition, it can accurately quantify the difference in energy levels between the ground and photoexcited states.[39] It is common knowledge that PL intensity is a key to pointing out the recombination behavior of photoinduced electron–hole (e^-/h^+) pairs. The e^-/h^+ separation in less time will occur with high PL intensities (*i.e.*, higher recombination rate), while the longer separation time is generally related to lower intensities (low recombination rate). That is a major feature for photocatalytic reactions.[64] In Fig. 6b, the PL spectra of three ZIFs were measured with an excitation wavelength of 310 nm at room temperature. All ZIF-8 materials reveal similar broad emission spectra in a wavelength range of 403–443 nm with a maximum peak at 422 nm. This peak might be driven by the photoinduced electron transitions from CB (lowest unoccupied molecular orbital, LUMO) to VB (highest occupied molecular orbital, HOMO) in ZIF-8 photocatalysts.[65,66] Among three catalysts, ZIF-8-F3 has the lowest PL intensity, signifying a longer e^-/h^+ separation time, which demonstrates higher photocatalytic efficiency on the leaf-like ZIF materials. This result yields the prolonged exciting states of charge carriers which can dissociate on the surface of ZIF-8-F3. Therefore, the photoinduced charge carriers tend to favor ZIF-8-F3 in the photodegradation of RB5 molecules. As a result, these obtained findings confirmed the efficient inhibition of the e^-/h^+ recombination and the higher charge migration in ZIF-8-F3 for effectively stimulating photocatalytic degradation.[39,67]

To gain a better understanding of the photocatalytic mechanism, the photoelectrochemical properties of three ZIF-8 materials were also examined. Furthermore, these properties can reveal the intrinsic reasons for enhancing the photocatalytic performance of materials.[68] The characteristics of ZIFs were explored by measuring their electrochemical impedance spectroscopic (EIS) responses and transient photocurrent (PC)

density under a UV beam. As known, the migration rate of charges plays a key role in photocatalytic reactions, which can be easily evaluated by EIS measurements.[69] Under 365 nm UV irradiation, as seen in Fig. 7a, the arc radius of ZIF-8-F3 (black curve) on the EIS Nyquist plot in the high-frequency region is the smallest, suggesting the transfer of interfacial charge carriers is the fastest among three ZIFs.[70] This result further indicates the more-effective separation of photogenerated e^-/h^+ pairs and faster interfacial charge migration for the layered ZIF-8-F3 materials. That makes the number of photogenerated charges increase as well as its photocatalytic activity. Besides that, the EIS performance of ZIF-8-F3 was also measured in the dark, and the result shows much larger migration resistance of charges than in UV conditions (its radius is rather large). This exploration reveals that the transfer efficiency of charge carriers is better when UV light is applied, meaning higher photocatalytic activity. With a similar tendency, high PC density shows the high separation efficiency of the photogenerated e^-/h^+ pairs.[68,71] As seen in Fig. 7b, three ZIF-8 samples display rapid PC responses upon the light being turned on or off, and the PC density of three ZIF samples remained nearly constant during the irradiation process. Such constancy was well-repeated in each on–off cycle. That proved the good reproducibility of the ZIF-8 materials. ZIF-8-F2 exhibits a minimum PC density, while ZIF-8-F3 shows the strongest response of approximately 1.7 times. This demonstrates that the separation efficiency of e^-/h^+ pairs in ZIF-8-F3 is the best.

In order to determine which reason caused the strong PC response of ZIF-8-F3 and also the role of irradiation wavelength in its photocatalytic reaction, the photocatalytic activity of three ZIF samples was measured under different monochromatic light irradiations of 365, 500, and 600 nm for 60 min (Fig. 7c). In the visible light region (>400 nm), ZIF-8-F3 showed a low removal efficiency of RB5, while this leaf-like material displayed the highest degradation of RB5 dye under 365 nm UV light of more than 12.5 times if compared to under irradiated wavelength of 600 nm. This can not only enhance the separation efficiency of e^-/h^+ pairs but also increase the photoexcited e^-/h^+
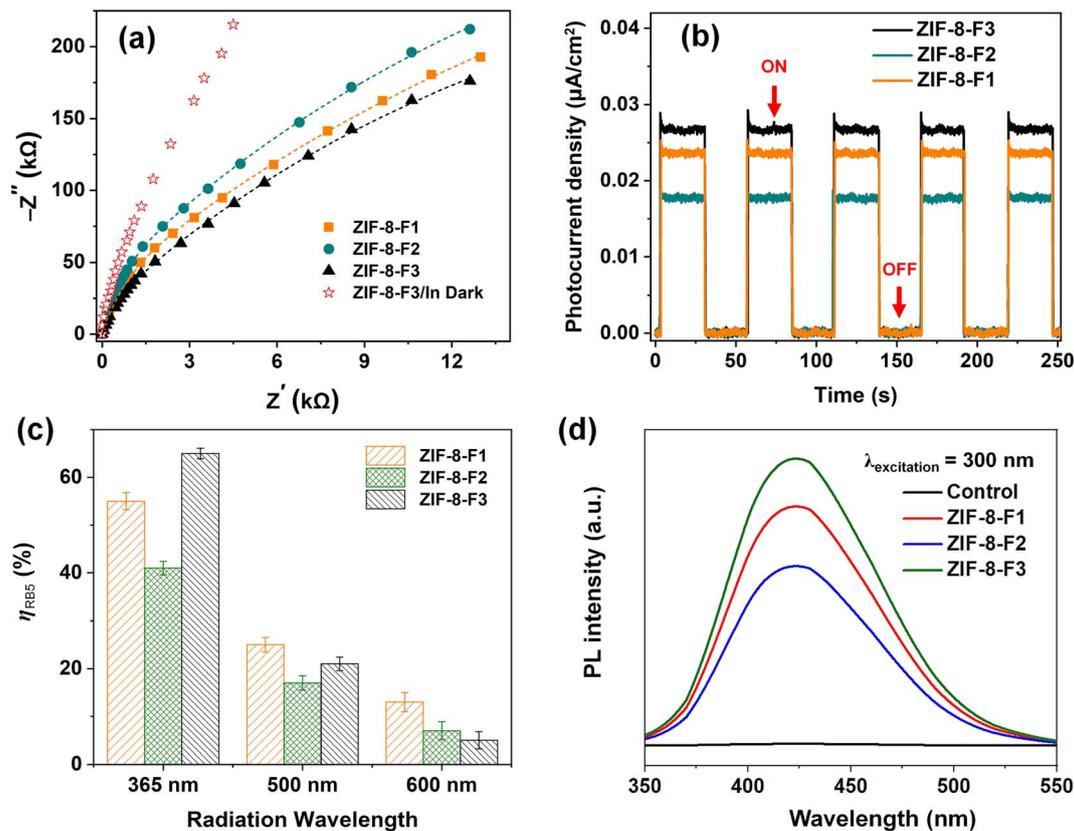
Fig. 7 (a) The Nyquist plot of EIS and (b) transient PC responses of ZIF-8 materials under UV irradiation. (c) The RB5 removal efficiency of three ZIF-8 photocatalysts under monochromatic light radiation wavelengths. (d) Fluorescence spectra of terephthalic acid in the absence or presence of three ZIF-8 samples.

pairs under UV light, hence resulting in a stronger PC response (*i.e.*, better photodegradation of RB5). In another investigation, the active species for the degradation of RB5 dye are hydroxyl ($\cdot$OH) radicals, which crucially affect the photocatalytic efficiency, and those radicals can also be probed by the fluorescence intensity measurement of terephthalic acid (1.0 mM) excited at 300 nm for 10 min.[72] The PL intensity of terephthalic acid with the synergistic presence of the ZIF-8 materials (0.5 g L^{-1}) under UV radiation revealed the emission peak at a wavelength of 425 nm (Fig. 7d), whereas it was typically characterless if there were no catalysts (black line). The peak intensity of three ZIF-8 materials was rapidly increased within 10 min due to the self-production of fluorescent 2-hydroxyterephthalic acid in post-irradiated solutions, implying that these ZIFs could favor the formation of $\cdot$OH radicals under UV light.[73] This phenomenon is attributed to the synergistic effect of ZIF-8 with a UV source. Furthermore, with the highest PL intensity for ZIF-8-F3, it can be clearly shown that 2D leaf-like ZIF-8 materials produce $\cdot$OH radicals more effectively than the others, suggesting their greater photocatalytic efficiency under UV irradiation.

According to the above-demonstrated results, it is revealed that the leaf-like ZIF-8 materials are superior in the photodegradation activity of RB5 dye to the other morphological two. Subsequently, ZIF-8-F3 will be used for further investigations.

The scavengers were applied to determine the role of active oxygen species in the photocatalytic degradation of RB5 dye under a 365 nm UV beam for 120 min, which can properly propose its possible degradation pathway.[38,39,74] All scavengers
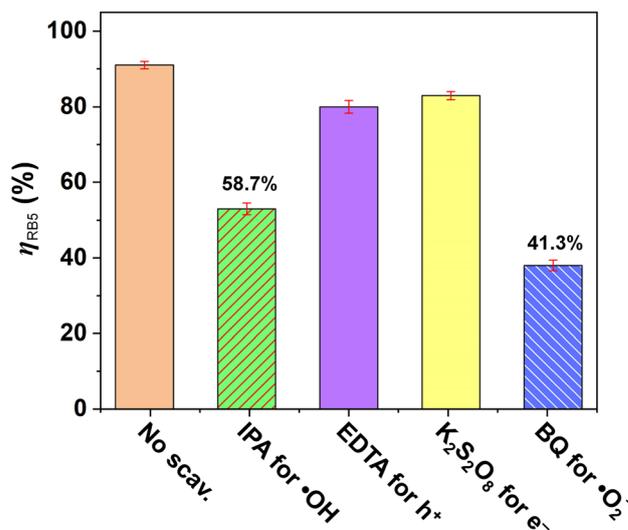

Fig. 8 The effect of different quenchers on the photocatalytic activity of leaf-like ZIF-8-F3 materials for RB5 degradation under 365 nm UV light.

were tested at the same concentration (1.0 mM), with 1.0 g L^{-1} of ZIF-8-F3 catalyst and 20 mg L^{-1} of aqueous RB5 solution at pH = 7.0. In typical, isopropyl alcohol (IPA), ethylenediaminetetraacetic acid (EDTA), potassium persulfate (K$_2$S$_2$O$_8$), and 1,4-benzoquinone (BQ) were used for trapping ˙OH radicals, holes (h$^+$), electrons (e$^-$), and superoxide radical anions (˙O$_2^-$), respectively.[35,74,75] In Fig. 8, the photodegradation efficiency of RB5 was significantly reduced in comparison to "No scavenger" in the cases of IPA (58%) and BQ (41%), while the additions of EDTA and K$_2$S$_2$O$_8$ had little effect. According to the signals of scavengers on the removal efficiency of RB5, their inhibitor effect is arranged as BQ > IPA > EDTA > K$_2$S$_2$O$_8$ > No scavenger. The inhibition efficiency of EDTA and K$_2$S$_2$O$_8$ on the photocatalytic activity is 12% and 8%, respectively. That means h$^+$ and e$^-$ can involve certain influences in the reaction. Moreover, this study concludes that the ˙OH and ˙O$_2^-$ radicals play a crucial role in the photocatalysis of RB5 dye.

On the basis of the above-obtained analyses, the ˙OH and ˙O$_2^-$ radicals play a dominant role in the decolorization/photodegradation of the RB5 solution under UV light. The photocatalytic mechanism of the leaf-like ZIF-8-F3 materials was proposed as seen in Scheme 2 and eqn (3)–(13). In general, the photocatalytic process occurs between two bands of CB (electrons, LUMO) and VB (holes, HOMO).[76] It is known that the ZIF-8 structures contain a tetrahedral configuration of Zn$_4$N, in which LUMO is crucially formed from the empty 4p^0 orbitals of Zn, and HOMO is from the 2p^3 bonding orbitals of N.[77] Furthermore, XPS can also be used to determine the specific VB and CB values of photocatalysts.[48] The XPS VB spectrum indicated the VB edge (E_{VB}) of 2D leaf-like ZIF-8-F3 materials to be approximately 2.2 eV (see Fig. S3†), which is less than EH$_2$O/˙OH (2.38 eV vs. normal hydrogen electrode).[78] As a result, ˙OH radicals were formed by photogenerated holes (eqn (6) and

(11)). The CB value (E_{CB}) of ZIF-8-F3 is interpolated according to the formula $E_g = E_{VB} - E_{CB}$, where E_g is the bandgap of F3 materials (4.15 eV, see Fig. 6a), to be −1.95 eV, which is more negative than EO$_2$/·O$_2^-$ (−0.33 eV vs. Normal Hydrogen Electrode).[78] Hence, ˙O$_2^-$ radicals should be generated by photoinduced electrons with surface oxygen (eqn (7)). Consequently, ˙OH and ˙O$_2^-$ are the main reactive radicals for the photocatalysis of RB5 dye. Additionally, the DMPO spin-trapping electron paramagnetic resonance (EPR) spectra of ZIF-8 materials also show the presence of ˙OH and ˙O$_2^-$ radicals (Fig. S4†). They enhanced signals with the extension of irradiation time. Therefore, the mechanism for RB5 decolorization might have followed the following pathways. First, RB5 molecules were partially decolorized in the solution due to their self-photolysis (eqn (3), (8) and (12)), and this phenomenon was also proved in Fig. 5d in the dark and UV light with the absence of photocatalysts. Then, the photogenerated e$^-$/h$^+$ pairs were formed on the ZIF-8 surface under UV irradiation (eqn (4) and (5)). In the meantime, the process shifted from the degradation reaction in the solution to the surface reaction. The holes on the surface of catalysts reacted with H$_2$O to generate ˙OH radicals (eqn (6)).[79] Subsequently, electrons were able to jump from VB to CB in ZIF-8,[67] in order to combine with O$_2$ adsorbed on the surface of photocatalysts to produce ˙O$_2^-$ (eqn (7)), and some ˙O$_2^-$ radicals might generate ˙OH (eqn (9)–(11)).[80] Finally, ˙OH/˙O$_2^-$ or RB5 molecules could undergo the redox reactions around the catalytic centers to generate degraded products (eqn (12) and (13)). The proper decolorization/photodegradation pathway is expressed as follows:

$$RB5 \xrightarrow{h\nu} RB5^* \qquad (3)$$

$$ZIF\text{-}8 \xrightarrow{h\nu} ZIF\text{-}8^* \qquad (4)$$
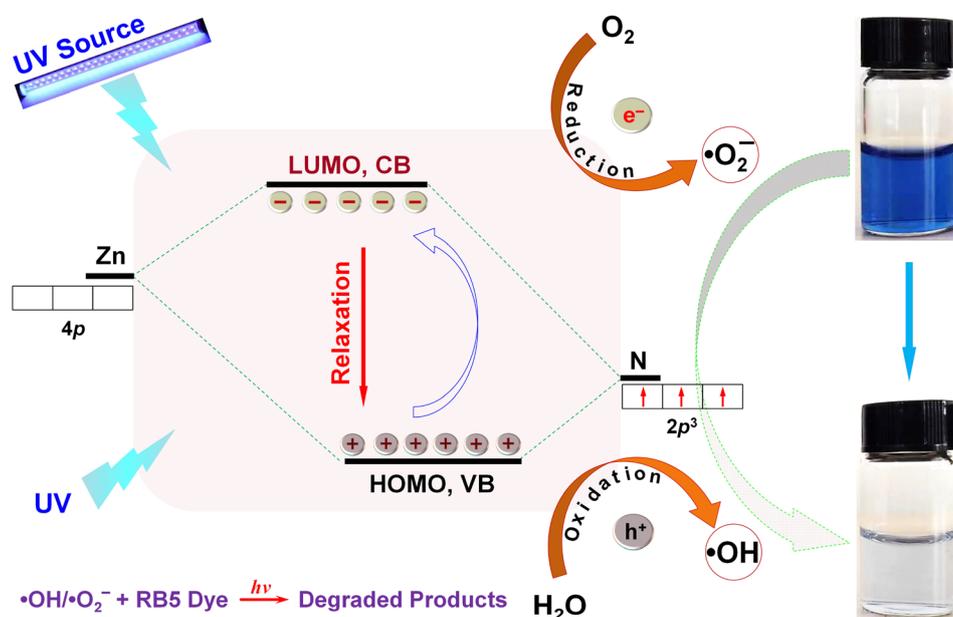
Scheme 2 The proposed mechanism for the photodegradation and decolorization of an aqueous RB5 solution by the ZIF-8 catalyst under UV irradiation.

$$ZIF\text{-}8^* \rightarrow h^+ + e^- \tag{5}$$

$$h^+ + H_2O \rightarrow H_2O^+ \rightarrow H^+ + {}^\cdot OH \tag{6}$$

$$e^- + O_2 \rightarrow {}^\cdot O_2^- \tag{7}$$

$$RB5^* + O_2 \rightarrow {}^\cdot RB5^+ + {}^\cdot O_2^- \tag{8}$$

$${}^\cdot O_2^- + 2H^+ + 2e^- \rightarrow H_2O_2 \tag{9}$$

$$H_2O_2 + e^- \rightarrow {}^\cdot OH + OH^- \tag{10}$$

$$OH^- + h^+ \rightarrow {}^\cdot OH \tag{11}$$

$${}^\cdot RB5^+ + H_2O \rightarrow \text{degraded products} + OH^- \tag{12}$$

$${}^\cdot OH/{}^\cdot O_2^- + RB5 \rightarrow \text{degraded products} \tag{13}$$
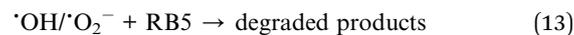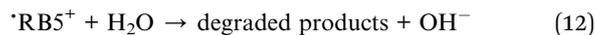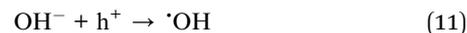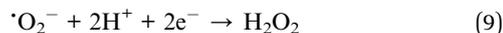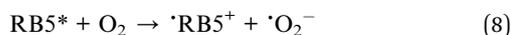
The photocatalytic influences of ZIF-8-F3 in the degradation of RB5 dye were investigated by varying the initial pH of the dye solution, the initial concentration of RB5, also the catalyst dosage in the dark for 50 min and under UV irradiation for
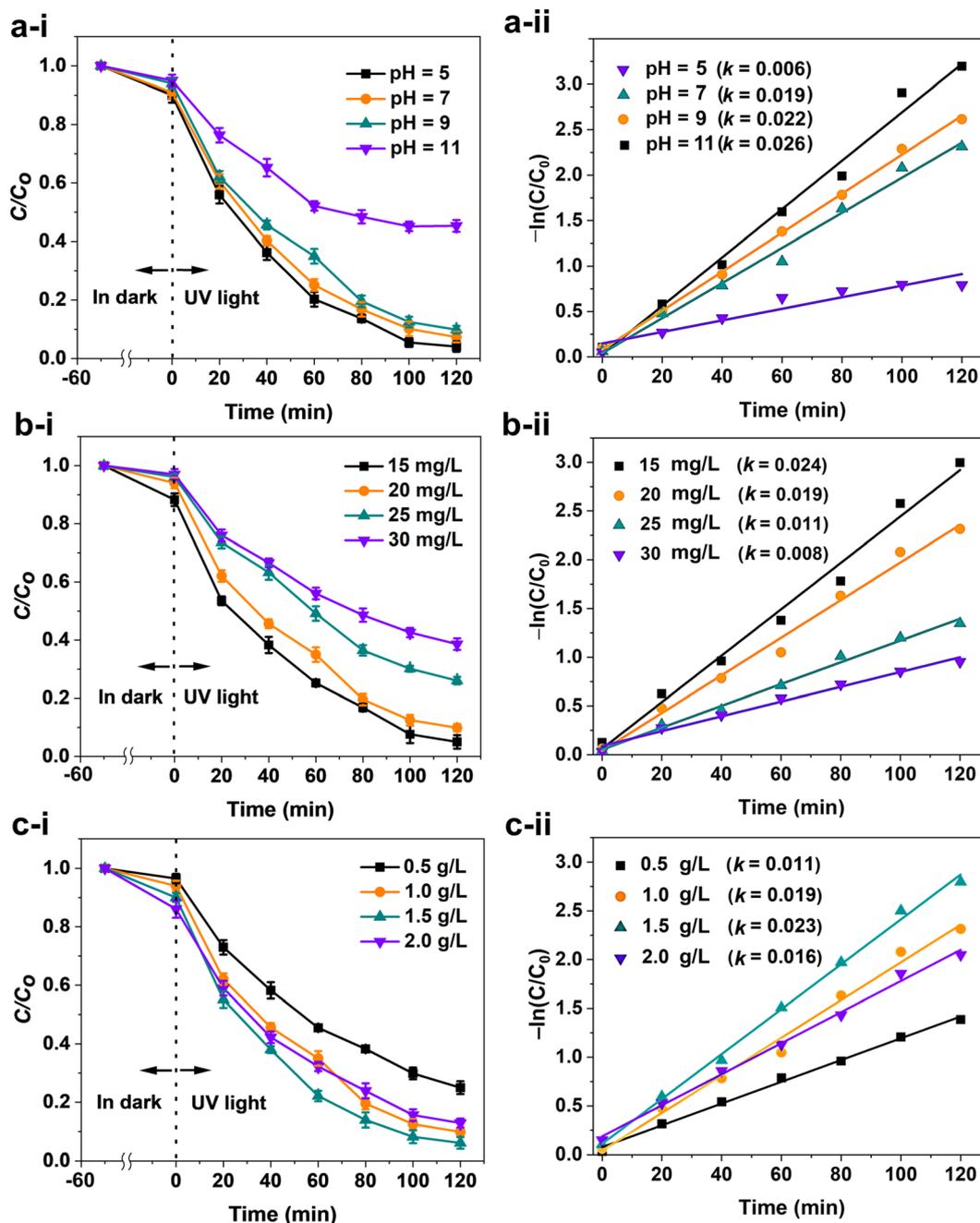
Fig. 9 Dependent graphs of C/C_0 vs. time (i) and their corresponding first-order plots (ii) for the degradation of RB5 dye by the ZIF-8-F3 material under UV irradiation in three different explorations: (a) initial pH, (b) initial RB5 concentration, and (c) used ZIF-8-F3 catalyst dosage.

120 min (Fig. 9). All results show that the degradation efficiency of RB5 was rather low in the dark for all explorations. In the first evaluation, the initial pH value of the RB5 solution is a pivotal factor that affects not only its photodegradation mechanism but also the decolorization rate due to the formation of charge carriers on the surface of catalysts or photogenerated ions.[81,82] In general, positive holes are generated at low pH, while $^\bullet$OH or $^\bullet O_2^-$ radicals are crucially responsible for the oxidation processes at a neutral or higher pH range.[83] The influence of the initial pH on the RB5 degradation under UV light was investigated with a pH range from 5 to 11, while the ZIF-8-F3 catalyst and RB5 dosages were constant at 1.0 g L^{-1} and 20 mg L^{-1}, respectively. It is clearly revealed that the dye removal efficiency increases when increasing the initial pH of RB5 (Fig. 9a-i). The photodegradation efficiency of RB5 reached 95% with pH = 11 after 120 min, while only 53% in a weakly acidic medium of pH = 5. As a result, their first-order rate constant increased with increasing pH values, reaching a maximum of 0.026 min^{-1} at pH = 11 (Fig. 9a-ii). Since the quantities of OH$^-$ ions increase in alkaline media (i.e., high pH), and definitely, the $^\bullet$OH species will be generated more (see eqn (10) and (11)). It is well corroborated that the $^\bullet$OH and $^\bullet O_2^-$ radicals are the major reactive oxygen species in the degradation reactions of RB5. Therefore, at a high pH of 11, the efficiency of photodegradation is clearly higher.[84,85]

In addition, the initial dye concentration is also another critical factor in the photodegradation reaction. At pH = 7, the impact of the initial RB5 content was investigated in a range of 15 to 30 mg L^{-1} in the presence of a 1.0 g L^{-1} ZIF-8-F3 catalyst. The corresponding results are shown in Fig. 9b. The dye degradation decreases when increasing the content of RB5 (Fig. 9b-i). It is clear that the dye solution was decolorized and the photocatalytic efficiency reached 93% for the initial RB5 concentration of 15 mg L^{-1}, while only 59% for a loading of 30 mg L^{-1}. Consequently, as seen in Fig. 9b-ii, the first-order rate constants of k increased progressively with decreasing RB5 content.[86] The rate constant k for the RB5 solution of 15 mg L^{-1} was 3.0 times higher than that of 30 mg L^{-1}. The degradation reduction can be attributed to the large adsorption

of the dye molecules on the surfaces of the catalyst at higher RB5 concentrations. In this way, it can largely hinder the interaction of UV irradiation with the catalyst (i.e., active sites), and probably the reactive $^\bullet$OH and $^\bullet O_2^-$ species are generated less, implying that the photocatalytic efficiency decreases. In the last investigation, the ZIF-8-F3 catalyst dosage was also examined for the photodegradation of 20 mg L^{-1} RB5 at pH = 7 (Fig. 9c). The dye removal efficiency reached 94% with a catalyst dosage of 1.5 g L^{-1} but only 74% for 0.5 g L^{-1} of ZIF-8-F3 (Fig. 9c-i). When the dosage was increased up to 2.0 g L^{-1}, however, the efficiency was only 85%. Besides, the first-order rate constant was the largest at 0.023 min^{-1} for a catalyst dosage of 1.5 g L^{-1} (Fig. 9c-ii). According to these results, the catalyst content loaded from 0.5 to 2.0 g L^{-1} has a not-too-large difference in the dye removal efficiency in comparison to the influences of the initial pH and RB5 concentration. In addition, the decrease in photodegradation (94 down to 85%) when increasing the catalyst dosages (1.5 up to 2.0 g L^{-1}) may come from the self-assembly/interaction between the catalyst particles and each other, which can form larger aggregates, hence decreasing not only the overall surface area but also the number of active sites. This study concluded that 1.5 g L^{-1} of ZIF-8-F3 photocatalyst is optimal for the degradation of 20 mg L^{-1} RB5 at pH = 7.

To investigate the stability and recyclability of the 2D leaf-like ZIF-8-F3 catalyst in the photodegradation of RB5 dye, five cycles of the dye removal were employed under 365 nm UV irradiation. The solid samples after photocatalytic reactions were cleaned with DI water several times, then completely oven-dried and used for the next runs. As shown in Fig. 10a, after five cycles, ZIF-8-F3 revealed a slight reduction of ~3.27% in photocatalytic activity. This can be attributed to a loss during the recycling process of the catalyst. Furthermore, the XRD results of ZIF-8-F3 before and after five cycles were also studied to evaluate their crystalline structures. As a clear result, the structure of the catalyst had no change and was similar to the original sample (Fig. 10b). This investigation shows that ZIF-8-F3 is a potential 2D material in the photocatalytic degradation of RB5 dye due to its high photostability and efficient
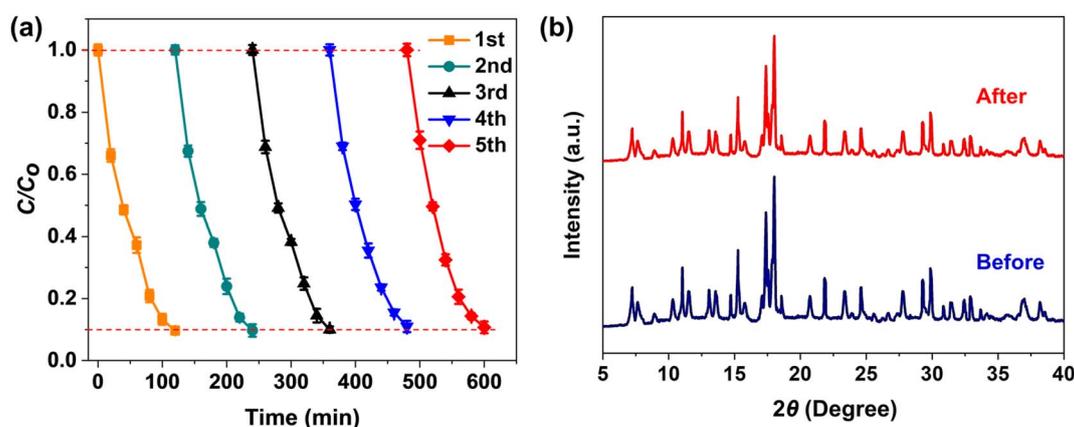

Fig. 10 (a) The reusability and (b) the XRD spectra of ZIF-8-F3 after five recycling runs. The initial concentrations of ZIF-8-F3 and RB5 are 1.0 g L^{-1} and 20 mg L^{-1} at pH = 7.0, respectively.

reusability. In addition, the as-synthetic ZIF-8-F3 photocatalyst is also a good 2D material for RB5 removal under UV light irradiation (see Table 2).

4. Conclusion

In summary, we successfully synthesized three ZIF-8 materials with different morphologies, including rhombic dodecahedral, pitaya-like, and leaf-like at ambient conditions from zinc clusters and 2-methylimidazole by altering the volume ratio of methanol and water assigned as a solvent. Although all three ZIFs showed efficient photocatalytic activity, the 2D leaf-like ZIF-8 still revealed the most efficiency in the decolorization of RB5 dye under 365 nm UV irradiation. This was due to the efficient inhibition of the electrons–holes recombination and the higher migration of charge carriers in ZIF-8-F3, hence producing more reactive $\cdot OH$ and $\cdot O_2^-$ species, meaning greater photocatalytic efficiency. In a neutral medium pH = 7, about 91% of the RB5 concentration was successfully photodegraded within 2 h with the presence of 1.0 g L^{-1} of ZIF-8-F3. The RB5 removal by this ZIF-8 was fitted by a pseudo-first-order kinetic model with an obtained rate constant k of 0.019 min^{-1}. Furthermore, when the effects of pH, initial dye content, and catalyst dosage were investigated, it was discovered that ZIF-8-F3 could work rather efficiently in alkaline media (typically pH = 11), with an initial RB5 concentration of 15 mg L^{-1} or a photocatalyst dosage of 1.5 g L^{-1}. The as-prepared ZIF-8-F3 materials had high reusability and photostability. So, in the future, 2D materials based on metal–organic frameworks might be thought of as a great photocatalyst for breaking down reactive black 5 dye, which could be useful for a number of promising applications in environmental remediation.

Author contributions

Conception and design of the study; acquisition of data; analysis and interpretation of data: L. G. T. (lgtrung@yu.ac.kr); M. K. N. (kimminhdn@gmail.com); T. D. H. N. (ntdhang@dut.udn.vn); V. A. T. (tavy@ntt.edu.vn); J. S. G. (sweat3000@ynu.ac.kr); N. T. T. (trannguyentien@duytan.edu.vn); drafting of paper (L. G. T., M. K. N., J. S. G., N. T. T.); critical revision for important content (L. G. T., M. K. N., J. S. G., N. T. T.). Final approval of the submitted version of the paper (L. G. T., M. K. N., J. S. G., N. T. T).

Conflicts of interest

The authors declare no competing financial interests or personal relationships that could have appeared to influence the work reported in this paper.

Acknowledgements

References

1 C. J. Vörösmarty, P. B. McIntyre, M. O. Gessner, D. Dudgeon, A. Prusevich, P. Green, S. Glidden, S. E. Bunn, C. A. Sullivan, C. R. Liermann and P. M. Davies, Erratum: Global Threats to Human Water Security and River Biodiversity, *Nature*, 2010, **468**(7321), 334, DOI: 10.1038/nature09549.

2 L. Schweitzer and J. Noblet, Chapter 3.6 - Water Contamination and Pollution, in *Green Chemistry*, ed. B. Török and T. B. T.-G. C. Dransfield, Elsevier, 2018, pp. 261–290, DOI: 10.1016/B978-0-12-809270-5.00011-X.

3 W. Liang, B. Wang, J. Cheng, D. Xiao, Z. Xie and J. Zhao, 3D, Eco-Friendly Metal-Organic Frameworks@carbon Nanotube Aerogels Composite Materials for Removal of Pesticides in Water, *J. Hazard. Mater.*, 2021, **401**, 123718, DOI: 10.1016/j.jhazmat.2020.123718.

4 L. Joseph, B.-M. Jun, M. Jang, C. M. Park, J. C. Muñoz-Senmache, A. J. Hernández-Maldonado, A. Heyden, M. Yu and Y. Yoon, Removal of Contaminants of Emerging Concern by Metal-Organic Framework Nanoadsorbents: A Review, *Chem. Eng. J.*, 2019, **369**, 928–946, DOI: 10.1016/j.cej.2019.03.173.

5 A. K. Verma, R. R. Dash and P. Bhunia, A Review on Chemical Coagulation/Flocculation Technologies for Removal of Colour from Textile Wastewaters, *J. Environ. Manage.*, 2012, **93**(1), 154–168, DOI: 10.1016/j.jenvman.2011.09.012.

6 G. Montes-Hernandez, N. Concha-Lozano, F. Renard and E. Quirico, Removal of Oxyanions from Synthetic Wastewater *via* Carbonation Process of Calcium Hydroxide: Applied and Fundamental Aspects, *J. Hazard. Mater.*, 2009, **166**(2), 788–795, DOI: 10.1016/j.jhazmat.2008.11.120.

7 S. Dong, J. Feng, M. Fan, Y. Pi, L. Hu, X. Han, M. Liu, J. Sun and J. Sun, Recent Developments in Heterogeneous Photocatalytic Water Treatment Using Visible Light-Responsive Photocatalysts: A Review, *RSC Adv.*, 2015, **5**(19), 14610–14630, DOI: 10.1039/C4RA13734E.

8 G. Ren, H. Han, Y. Wang, S. Liu, J. Zhao, X. Meng and Z. Li, Recent Advances of Photocatalytic Application in Water Treatment: A Review, *Nanomaterials*, 2021, **11**(7), 1804, DOI: 10.3390/nano11071804.

9 Z. Li, X. Meng and Z. Zhang, Fabrication of Surface Hydroxyl Modified g-C_3N_4 with Enhanced Photocatalytic Oxidation Activity, *Catal. Sci. Technol.*, 2019, **9**(15), 3979–3993, DOI: 10.1039/C9CY00550A.

10 K. Wang, B. Li, C. Zhao, S. Yuan, C. Zhang, X. Liang, J. Wang, Y. Wu and Y. He, A Novel NiO/BaTiO(3) Heterojunction for Piezocatalytic Water Purification under Ultrasonic Vibration, *Ultrason. Sonochem.*, 2023, **92**, 106285, DOI: 10.1016/j.ultsonch.2022.106285.

11 S. Zheng, X. Li, J. Zhang, J. Wang, C. Zhao, X. Hu, Y. Wu and Y. He, One-Step Preparation of MoOx/ZnS/ZnO Composite and Its Excellent Performance in Piezocatalytic Degradation of Rhodamine B under Ultrasonic Vibration,

J. Environ. Sci., 2023, **125**, 1–13, DOI: 10.1016/j.jes.2021.10.028.

12 S. Tu, Y. Guo, Y. Zhang, C. Hu, T. Zhang, T. Ma and H. Huang, Piezocatalysis and Piezo-Photocatalysis: Catalysts Classification and Modification Strategy, Reaction Mechanism, and Practical Application, *Adv. Funct. Mater.*, 2020, **30**(48), 2005158, DOI: 10.1002/adfm.202005158.

13 C. Zhao, L. Cai, K. Wang, B. Li, S. Yuan, Z. Zeng, L. Zhao, Y. Wu and Y. He, Novel Bi_2WO_6/$ZnSnO_3$ Heterojunction for the Ultrasonic-Vibration-Driven Piezocatalytic Degradation of RhB, *Environ. Pollut.*, 2023, **319**, 120982, DOI: 10.1016/j.envpol.2022.120982.

14 N. T. Tran, D. Kim, K. S. Yoo and J. Kim, Synthesis of Cu-Doped MOF-235 for the Degradation of Methylene Blue under Visible Light Irradiation, *Bull. Korean Chem. Soc.*, 2019, **40**(2), 112–117, DOI: 10.1002/bkcs.11650.

15 N. T. Tran, L. G. Trung and M. K. Nguyen, The Degradation of Organic Dye Contaminants in Wastewater and Solution from Highly Visible Light Responsive ZIF-67 Monodisperse Photocatalyst, *J. Solid State Chem.*, 2021, **300**, 122287, DOI: 10.1016/j.jssc.2021.122287.

16 N. T. Tran, H. T. Kwon, W.-S. Kim and J. Kim, Counter-Diffusion-Based *In Situ* Synthesis of ZIF-67 Membranes for Propylene/Propane Separation, *Mater. Lett.*, 2020, **271**, 127777, DOI: 10.1016/j.matlet.2020.127777.

17 M. K. Nguyen, L. G. Trung, H. H. Nguyen and N. T. Tran, Preparation of $Al(OH)_3$-Based Layered Structural Material by Shear Alignment from Aqueous Dispersion of Colloidal Gibbsite Platelets, *J. Taiwan Inst. Chem. Eng.*, 2021, **125**, 332–339, DOI: 10.1016/j.jtice.2021.06.006.

18 L. G. Trung, S. Subedi, A. K. Rella, V. Kumar and S.-W. Kang, Folding-Induced in-Plane Birefringence in Homeotropically Aligned Graphene-Oxide Liquid Crystal Films Formed by Solution Shear, *Liq. Cryst.*, 2022, **49**(3), 407–417, DOI: 10.1080/02678292.2021.1974585.

19 L. G. Trung, S. Subedi, B. Dahal, P. L. Truong, J. S. Gwag, N. T. Tran and M. K. Nguyen, Highly Efficient Fluorescent Probes from Chitosan-Based Amino-Functional Carbon Dots for the Selective Detection of Cu^{2+} Traces, *Mater. Chem. Phys.*, 2022, **291**, 126772, DOI: 10.1016/j.matchemphys.2022.126772.

20 N. T. Tran, T. K. Vo, J. Kim and M. R. Othman, Esoteric CO Adsorption by $CuCl$-$NiCl_2$ Embedded Microporous MIL-101 (Cr), *Colloids Surf., A*, 2021, **615**, 126242.

21 N. T. Tran, T. Yu, J. Kim and M. Othman, ZIF-8 Tubular Membrane for Propylene Purification: Effect of Surface Curvature and Zinc Salts on Separation Performance, *Sep. Purif. Technol.*, 2020, **251**, 117354, DOI: 10.1016/j.seppur.2020.117354.

22 J. Li, H. Wang, X. Yuan, J. Zhang and J. W. Chew, Metal-Organic Framework Membranes for Wastewater Treatment and Water Regeneration, *Coord. Chem. Rev.*, 2020, **404**, 213116, DOI: 10.1016/j.ccr.2019.213116.

23 S. Chao, X. Li, Y. Li, Y. Wang and C. Wang, Preparation of Polydopamine-Modified Zeolitic Imidazolate Framework-8 Functionalized Electrospun Fibers for Efficient Removal of Tetracycline, *J. Colloid Interface Sci.*, 2019, **552**, 506–516, DOI: 10.1016/j.jcis.2019.05.078.

24 J. Yao and H. Wang, Zeolitic Imidazolate Framework Composite Membranes and Thin Films: Synthesis and Applications, *Chem. Soc. Rev.*, 2014, **43**(13), 4470–4493, DOI: 10.1039/C3CS60480B.

25 Y. Feng, H. Wang and J. Yao, Synthesis of 2D Nanoporous Zeolitic Imidazolate Framework Nanosheets for Diverse Applications, *Coord. Chem. Rev.*, 2021, **431**, 213677, DOI: 10.1016/j.ccr.2020.213677.

26 N. Hassan, A. Shahat, A. El-Didamony, M. G. El-Desouky and A. A. El-Bindary, Synthesis and Characterization of ZnO Nanoparticles *via* Zeolitic Imidazolate Framework-8 and Its Application for Removal of Dyes, *J. Mol. Struct.*, 2020, **1210**, 128029, DOI: 10.1016/j.molstruc.2020.128029.

27 X.-C. Huang, Y.-Y. Lin, J.-P. Zhang and X.-M. Chen, Ligand-Directed Strategy for Zeolite-Type Metal–Organic Frameworks: Zinc(II) Imidazolates with Unusual Zeolitic Topologies, *Angew. Chem., Int. Ed.*, 2006, **45**(10), 1557–1559, DOI: 10.1002/anie.200503778.

28 P. K. Sung, N. Zheng, P. C. Adrien, C. J. Yong, H. Rudan, J. U.-R. Fernando, K. C. Hee, O. Michael and M. Y. Omar, Exceptional Chemical and Thermal Stability of Zeolitic Imidazolate Frameworks, *Proc. Natl. Acad. Sci. U. S. A.*, 2006, **103**(27), 10186–10191, DOI: 10.1073/pnas.0602439103.

29 S. R. Venna, J. B. Jasinski and M. A. Carreon, Structural Evolution of Zeolitic Imidazolate Framework-8, *J. Am. Chem. Soc.*, 2010, **132**(51), 18030–18033, DOI: 10.1021/ja109268m.

30 R. Banerjee, A. Phan, B. Wang, C. Knobler, H. Furukawa, M. O'Keeffe and O. M. Yaghi, High-Throughput Synthesis of Zeolitic Imidazolate Frameworks and Application to CO_2 Capture, *Science*, 2008, **319**(5865), 939–943, DOI: 10.1126/science.1152516.

31 N. Tran, J. Kim and M. Othman, Microporous ZIF-8 Membrane Prepared from Secondary Growth for Improved Propylene Permeance and Selectivity, *Microporous Mesoporous Mater.*, 2019, **285**, 178–184, DOI: 10.1016/j.micromeso.2019.05.010.

32 K. Sahel, N. Perol, H. Chermette, C. Bordes, Z. Derriche and C. Guillard, Photocatalytic Decolorization of Remazol Black 5 (RB5) and Procion Red MX-5B—Isotherm of Adsorption, Kinetic of Decolorization and Mineralization, *Appl. Catal., B*, 2007, **77**(1), 100–109, DOI: 10.1016/j.apcatb.2007.06.016.

33 S. K. Kansal, N. Kaur and S. Singh, Photocatalytic Degradation of Two Commercial Reactive Dyes in Aqueous Phase Using Nanophotocatalysts, *Nanoscale Res. Lett.*, 2009, **4**(7), 709, DOI: 10.1007/s11671-009-9300-3.

34 E. K. Goharshadi, M. Hadadian, M. Karimi and H. Azizi-Toupkanloo, Photocatalytic Degradation of Reactive Black 5 Azo Dye by Zinc Sulfide Quantum Dots Prepared by a Sonochemical Method, *Mater. Sci. Semicond. Process.*, 2013, **16**(4), 1109–1116, DOI: 10.1016/j.mssp.2013.03.005.

35 M. S. Lucas, P. B. Tavares, J. A. Peres, J. L. Faria, M. Rocha, C. Pereira and C. Freire, Photocatalytic Degradation of Reactive Black 5 with TiO_2-Coated Magnetic Nanoparticles,

Catal. Today, 2013, **209**, 116–121, DOI: 10.1016/j.cattod.2012.10.024.

36 N. A. H. M. Nordin, A. F. Ismail, A. Mustafa, P. S. Goh, D. Rana and T. Matsuura, Aqueous Room Temperature Synthesis of Zeolitic Imidazole Framework 8 (ZIF-8) with Various Concentrations of Triethylamine, *RSC Adv.*, 2014, **4**(63), 33292–33300, DOI: 10.1039/C4RA03593C.

37 X. Li, Z. Li, L. Lu, L. Huang, L. Xiang, J. Shen, S. Liu and D.-R. Xiao, The Solvent Induced Inter-Dimensional Phase Transformations of Cobalt Zeolitic-Imidazolate Frameworks, *Chem. - Eur. J.*, 2017, **23**(44), 10638–10643, DOI: 10.1002/chem.201701721.

38 S. Angela, V. Bervia Lunardi, K. Kusuma, F. Edi Soetaredjo, J. Nyoo Putro, S. Permatasari Santoso, A. Elisa Angkawijaya, J. Lie, C. Gunarto, A. Kurniawan and S. Ismadji, Facile Synthesis of Hierarchical Porous ZIF-8@TiO$_2$ for Simultaneous Adsorption and Photocatalytic Decomposition of Crystal Violet, *Environ. Nanotechnol., Monit. Manage.*, 2021, **16**, 100598, DOI: 10.1016/j.enmm.2021.100598.

39 K. C. Devarayapalli, S. V. P. Vattikuti, T. V. M. Sreekanth, K. S. Yoo, P. C. Nagajyothi and J. Shim, Hydrogen Production and Photocatalytic Activity of g-C$_3$N$_4$/Co-MOF (ZIF-67) Nanocomposite under Visible Light Irradiation, *Appl. Organomet. Chem.*, 2020, **34**(3), e5376, DOI: 10.1002/aoc.5376.

40 G. Gong, Y. Liu, B. Mao, B. Wang, L. Tan, D. Li, Y. Liu and W. Shi, Mechanism Study on the Photocatalytic Efficiency Enhancement of MoS$_2$ Modified Zn–AgIn5S8 Quantum Dots, *RSC Adv.*, 2016, **6**(101), 99023–99033, DOI: 10.1039/C6RA19949F.

41 D. Wang, X. Li, J. Chen and X. Tao, Enhanced Photoelectrocatalytic Activity of Reduced Graphene Oxide/TiO$_2$ Composite Films for Dye Degradation, *Chem. Eng. J.*, 2012, **198–199**, 547–554, DOI: 10.1016/j.cej.2012.04.062.

42 L. G. Trung, R. K. Mishra, S. Subedi, A. K. Rella, V. Kumar, J. W. Ryu, H. Jeon and J. S. Gwag, Graphene Oxide Liquid Crystals Aligned in a Confined Configuration: Implications for Optical Materials, *ACS Appl. Nano Mater.*, 2022, **5**(8), 11506–11518, DOI: 10.1021/acsanm.2c02537.

43 C. Shuai, X. Yuan, Y. Shuai, G. Qian, J. Yao, W. Xu, S. Peng and W. Yang, Nitrogen-Doped Carbon-ZnO Heterojunction Derived from ZIF-8: A Photocatalytic Antibacterial Strategy for Scaffold, *Mater. Today Nano*, 2022, **18**, 100210, DOI: 10.1016/j.mtnano.2022.100210.

44 A. Deacon, L. Briquet, M. Malankowska, F. Massingberd-Mundy, S. Rudić, T. l. Hyde, H. Cavaye, J. Coronas, S. Poulston and T. Johnson, Understanding the ZIF-L to ZIF-8 Transformation from Fundamentals to Fully Costed Kilogram-Scale Production, *Commun. Chem.*, 2022, **5**(1), 18, DOI: 10.1038/s42004-021-00613-z.

45 S. M. Marji, M. F. Bayan and A. Jaradat, Facile Fabrication of Methyl Gallate Encapsulated Folate ZIF-L Nanoframeworks as a PH Responsive Drug Delivery System for Anti-Biofilm and Anticancer Therapy, *Biomimetics*, 2022, **7**(4), 242, DOI: 10.3390/biomimetics7040242.

46 B. Liu, M. Jian, R. Liu, J. Yao and X. Zhang, Highly Efficient Removal of Arsenic(III) from Aqueous Solution by Zeolitic Imidazolate Frameworks with Different Morphology, *Colloids Surf., A*, 2015, **481**, 358–366, DOI: 10.1016/j.colsurfa.2015.06.009.

47 Y. Wu, M. Zhou, B. Zhang, B. Wu, J. Li, J. Qiao, X. Guan and F. Li, Amino Acid Assisted Templating Synthesis of Hierarchical Zeolitic Imidazolate Framework-8 for Efficient Arsenate Removal, *Nanoscale*, 2014, **6**(2), 1105–1112, DOI: 10.1039/C3NR04390H.

48 Y. Pan, W. Liu, Y. Zhao, C. Wang and Z. Lai, Improved ZIF-8 Membrane: Effect of Activation Procedure and Determination of Diffusivities of Light Hydrocarbons, *J. Membr. Sci.*, 2015, **493**, 88–96, DOI: 10.1016/j.memsci.2015.06.019.

49 J. Cravillon, S. Münzer, S.-J. Lohmeier, A. Feldhoff, K. Huber and M. Wiebcke, Rapid Room-Temperature Synthesis and Characterization of Nanocrystals of a Prototypical Zeolitic Imidazolate Framework, *Chem. Mater.*, 2009, **21**(8), 1410–1412, DOI: 10.1021/cm900166h.

50 M. S. Lucas and J. A. Peres, Decolorization of the Azo Dye Reactive Black 5 by Fenton and Photo-Fenton Oxidation, *Dyes Pigm.*, 2006, **71**(3), 236–244, DOI: 10.1016/j.dyepig.2005.07.007.

51 J. G. Goodwin Jr, S. Kim and W. D. Rhodes, Turnover Frequencies in Metal Catalysis: Meanings, Functionalities and Relationships, in *Catalysis*, ed. J. J. Spivey and G. W. Roberts, The Royal Society of Chemistry, 2004, vol. 17, pp. 320–348, DOI: 10.1039/9781847553294-00320.

52 R. Kamaludin, M. H. D. Othman, S. H. S. A. Kadir, A. F. Ismail, M. A. Rahman and J. Jaafar, Visible-Light-Driven Photocatalytic N-Doped TiO2 for Degradation of Bisphenol A (BPA) and Reactive Black 5 (RB5) Dye, *Water, Air, Soil Pollut.*, 2018, **229**(11), 363, DOI: 10.1007/s11270-018-4006-8.

53 M. Oveisi, M. Alinia Asli and N. M. Mahmoodi, Carbon Nanotube Based Metal-Organic Framework Nanocomposites: Synthesis and Their Photocatalytic Activity for Decolorization of Colored Wastewater, *Inorg. Chim. Acta*, 2019, **487**, 169–176, DOI: 10.1016/j.ica.2018.12.021.

54 Z. Lan, C. Wang and J. Qu, In-Situ Growth of ZIF-8 Nanocrystals to Prepare Cotton-Based Composites with Dye Degradation and Antibacterial Abilities, *Mater. Res. Bull.*, 2019, **116**, 40–43, DOI: 10.1016/j.materresbull.2019.04.009.

55 L. C. Ferreira, M. S. Lucas, J. R. Fernandes and P. B. Tavares, Photocatalytic Oxidation of Reactive Black 5 with UV-A LEDs, *J. Environ. Chem. Eng.*, 2016, **4**(1), 109–114, DOI: 10.1016/j.jece.2015.10.042.

56 S. Laohaprapanon, J. Matahum, L. Tayo and S.-J. You, Photodegradation of Reactive Black 5 in a ZnO/UV Slurry Membrane Reactor, *J. Taiwan Inst. Chem. Eng.*, 2015, **49**, 136–141, DOI: 10.1016/j.jtice.2014.11.017.

57 S. Song, L. Xu, Z. He, J. Chen, X. Xiao and B. Yan, Mechanism of the Photocatalytic Degradation of C.I. Reactive Black 5 at PH 12.0 Using SrTiO$_3$/CeO$_2$ as the Catalyst, *Environ. Sci. Technol.*, 2007, **41**(16), 5846–5853, DOI: 10.1021/es070224i.

58 D. K. Bhatt and U. D. Patel, Photocatalytic Degradation of Reactive Black 5 Using Ag$_3$PO$_4$ under Visible Light, *J. Phys. Chem. Solids*, 2021, **149**, 109768, DOI: **10.1016/j.jpcs.2020.109768**.

59 M. Karimi-Nazarabad and E. K. Goharshadi, Highly Efficient Photocatalytic and Photoelectrocatalytic Activity of Solar Light Driven WO$_3$/g-C$_3$N$_4$ Nanocomposite, *Sol. Energy Mater. Sol. Cells*, 2017, **160**, 484–493, DOI: **10.1016/j.solmat.2016.11.005**.

60 C. P. Wong, C. W. Lai, K. M. Lee and S. B. Hamid, Advanced Chemical Reduction of Reduced Graphene Oxide and Its Photocatalytic Activity in Degrading Reactive Black 5, *Materials*, 2015, **8**(10), 7118–7128, DOI: **10.3390/ma8105363**.

61 X. Yang, L. Qiu and X. Luo, ZIF-8 Derived Ag-Doped ZnO Photocatalyst with Enhanced Photocatalytic Activity, *RSC Adv.*, 2018, **8**(9), 4890–4894, DOI: **10.1039/C7RA13351K**.

62 H. Misran, N. Mahadi, S. Z. Othman, Z. Lockman, N. Amin and A. Matsumoto, Room Temperature Synthesis and Characterizations of ZIF-8 Formation at Water-Fatty Alcohols Interface, *J. Phys.: Conf. Ser.*, 2018, **1082**(1), 12046, DOI: **10.1088/1742-6596/1082/1/012046**.

63 X. Dai, X. Li, M. Zhang, J. Xie and X. Wang, Zeolitic Imidazole Framework/Graphene Oxide Hybrid Functionalized Poly(Lactic Acid) Electrospun Membranes: A Promising Environmentally Friendly Water Treatment Material, *ACS Omega*, 2018, **3**(6), 6860–6866, DOI: **10.1021/acsomega.8b00792**.

64 Q. Chen, R. Tong, X. Chen, Y. Xue, Z. Xie, Q. Kuang and L. Zheng, Ultrafine ZnO Quantum Dot-Modified TiO$_2$ Composite Photocatalysts: The Role of the Quantum Size Effect in Heterojunction-Enhanced Photocatalytic Hydrogen Evolution, *Catal. Sci. Technol.*, 2018, **8**(5), 1296–1303, DOI: **10.1039/C7CY02310C**.

65 X. Yan, K. Liu and W. Shi, Facile Synthesis of CdS/MnWO$_4$ Heterojunction with Enhanced Visible-Light-Driven Photocatalytic Activity and Mechanism Investigation, *Colloids Surf., A*, 2017, **520**, 138–145, DOI: **10.1016/j.colsurfa.2017.01.065**.

66 M. A. Nasalevich, M. van der Veen, F. Kapteijn and J. Gascon, Metal–Organic Frameworks as Heterogeneous Photocatalysts: Advantages and Challenges, *CrystEngComm*, 2014, **16**(23), 4919–4926, DOI: **10.1039/C4CE00032C**.

67 S. Panneri, M. Thomas, P. Ganguly, B. N. Nair, A. P. Mohamed, K. G. K. Warrier and U. S. Hareesh, C$_3$N$_4$ Anchored ZIF 8 Composites: Photo-Regenerable, High Capacity Sorbents as Adsorptive Photocatalysts for the Effective Removal of Tetracycline from Water, *Catal. Sci. Technol.*, 2017, **7**(10), 2118–2128, DOI: **10.1039/C7CY00348J**.

68 C. Yu, W. Zhou, L. Zhu, G. Li, K. Yang and R. Jin, Integrating Plasmonic Au Nanorods with Dendritic like α-Bi$_2$O$_3$/Bi$_2$O$_2$CO$_3$ Heterostructures for Superior Visible-Light-Driven Photocatalysis, *Appl. Catal., B*, 2016, **184**, 1–11, DOI: **10.1016/j.apcatb.2015.11.026**.

69 C. Lei, F. Han, D. Li, W.-C. Li, Q. Sun, X.-Q. Zhang and A.-H. Lu, Dopamine as the Coating Agent and Carbon Precursor for the Fabrication of N-Doped Carbon Coated Fe$_3$O$_4$ Composites as Superior Lithium Ion Anodes, *Nanoscale*, 2013, **5**(3), 1168–1175, DOI: **10.1039/C2NR33043A**.

70 X. Chen, F. Chen, F. Liu, X. Yan, W. Hu, G. Zhang, L. Tian, Q. Xia and X. Chen, Ag Nanoparticles/Hematite Mesocrystals Superstructure Composite: A Facile Synthesis and Enhanced Heterogeneous Photo-Fenton Activity, *Catal. Sci. Technol.*, 2016, **6**(12), 4184–4191, DOI: **10.1039/C6CY00080K**.

71 L. Di, H. Yang, T. Xian, X. Liu and X. Chen, Photocatalytic and Photo-Fenton Catalytic Degradation Activities of Z-Scheme Ag$_2$S/BiFeO$_3$ Heterojunction Composites under Visible-Light Irradiation, *Nanomaterials*, 2019, **9**(3), 399, DOI: **10.3390/nano9030399**.

72 M. Chin, C. Cisneros, S. M. Araiza, K. M. Vargas, K. M. Ishihara and F. Tian, Rhodamine B Degradation by Nanosized Zeolitic Imidazolate Framework-8 (ZIF-8), *RSC Adv.*, 2018, **8**(47), 26987–26997, DOI: **10.1039/C8RA03459A**.

73 V. A. Tran, A. N. Kadam and S.-W. Lee, Adsorption-Assisted Photocatalytic Degradation of Methyl Orange Dye by Zeolite-Imidazole-Framework-Derived Nanoparticles, *J. Alloys Compd.*, 2020, **835**, 155414, DOI: **10.1016/j.jallcom.2020.155414**.

74 P. Li, J. Li, X. Feng, J. Li, Y. Hao, J. Zhang, H. Wang, A. Yin, J. Zhou, X. Ma and B. Wang, Metal-Organic Frameworks with Photocatalytic Bactericidal Activity for Integrated Air Cleaning, *Nat. Commun.*, 2019, **10**(1), 2177, DOI: **10.1038/s41467-019-10218-9**.

75 M. Muruganandham and M. Swaminathan, Photocatalytic Decolourisation and Degradation of Reactive Orange 4 by TiO$_2$-UV Process, *Dyes Pigm.*, 2006, **68**(2), 133–142, DOI: **10.1016/j.dyepig.2005.01.004**.

76 C. Gao, J. Wang, H. Xu and Y. Xiong, Coordination Chemistry in the Design of Heterogeneous Photocatalysts, *Chem. Soc. Rev.*, 2017, **46**(10), 2799–2823, DOI: **10.1039/C6CS00727A**.

77 K. T. Butler, C. H. Hendon and A. Walsh, Electronic Chemical Potentials of Porous Metal–Organic Frameworks, *J. Am. Chem. Soc.*, 2014, **136**(7), 2703–2706, DOI: **10.1021/ja4110073**.

78 J. Liu, R. Li, Y. Hu, T. Li, Z. Jia, Y. Wang, Y. Wang, X. Zhang and C. Fan, Harnessing Ag Nanofilm as an Electrons Transfer Mediator for Enhanced Visible Light Photocatalytic Performance of Ag@AgCl/Ag Nanofilm/ZIF-8 Photocatalyst, *Appl. Catal., B*, 2017, **202**, 64–71, DOI: **10.1016/j.apcatb.2016.09.015**.

79 S. V. P. Vattikuti, P. A. K. Reddy, J. Shim and C. Byon, Visible-Light-Driven Photocatalytic Activity of SnO$_2$–ZnO Quantum Dots Anchored on g-C$_3$N$_4$ Nanosheets for Photocatalytic Pollutant Degradation and H$_2$ Production, *ACS Omega*, 2018, **3**(7), 7587–7602, DOI: **10.1021/acsomega.8b00471**.

80 Y. Huang, Y. Liang, Y. Rao, D. Zhu, J. Cao, Z. Shen, W. Ho and S. C. Lee, Environment-Friendly Carbon Quantum Dots/ZnFe$_2$O$_4$ Photocatalysts: Characterization, Biocompatibility, and Mechanisms for NO Removal, *Environ. Sci. Technol.*, 2017, **51**(5), 2924–2933, DOI: **10.1021/acs.est.6b04460**.

81 A. Dowling, R. Clift, N. Grobert, D. Hutton, R. Oliver, O. O'neill, J. Pethica, N. Pidgeon, J. Porritt, J. Ryan, *et al.*, Nanoscience and Nanotechnologies: Opportunities and Uncertainties, *London: R. Soc. R. Acad. Eng. Rep.*, 2004, **4**, 7–10, DOI: 10.1007/s00234-004-1255-6.

82 R. Chandra and M. Nath, Multi-Core–Shell TiO$_2$NPs@ZIF-8 Composite for Enhanced Photocatalytic Degradation and Adsorption of Methylene Blue and Rhodamine-B, *ChemistrySelect*, 2017, **2**(25), 7711–7722, DOI: 10.1002/slct.201701195.

83 A. Ajmal, I. Majeed, R. N. Malik, H. Idriss and M. A. Nadeem, Principles and Mechanisms of Photocatalytic Dye Degradation on TiO$_2$ Based Photocatalysts: A Comparative Overview, *RSC Adv.*, 2014, **4**(70), 37003–37026, DOI: 10.1039/C4RA06658H.

84 S. Yoon, J. J. Calvo and M. C. So, Removal of Acid Orange 7 from Aqueous Solution by Metal-Organic Frameworks, *Crystals*, 2019, **9**(1), 17, DOI: 10.3390/cryst9010017.

85 C. Liu, L.-Q. Yu, Y.-T. Zhao and Y.-K. Lv, Recent Advances in Metal-Organic Frameworks for Adsorption of Common Aromatic Pollutants, *Microchim. Acta*, 2018, **185**(7), 342, DOI: 10.1007/s00604-018-2879-2.

86 A. Abulizi, G.-H. Yang and J.-J. Zhu, One-Step Simple Sonochemical Fabrication and Photocatalytic Properties of Cu$_2$O–RGO Composites, *Ultrason. Sonochem.*, 2014, **21**(1), 129–135, DOI: 10.1016/j.ultsonch.2013.07.013.